Int. J. Electrochem. Sci., 14 **(2019)** 1658 – 1669, doi: 10.20964/2019.02.14

International Journal of
ELECTROCHEMICAL
SCIENCE
www.electrochemsci.org

Cadmium-based Coordination Polymer Nanorods and Microblocks as Anode Materials for Lithium-Ion Batteries

Yanyong Sha [1], *Changdong Shi*[1], *Yuanrui Gao*[2], *Hao Wen*[1], *Hongren Rong* [1], *Hong-Jiang Liu*[2,*], *Qi Liu*[1,3,*]

[1] School of Petrochemical Engineering and Jiangsu Key Laboratory of Fine Petro-chemical Technology, Changzhou University, 1 Gehu Road, Changzhou, Jiangsu 213164, P. R. China
[2] Department of Chemistry, College of Science, Shanghai University, No. 99 Shangda Road, Shanghai, 200444, P. R. China.
[3] State Key Laboratory of Coordination Chemistry, Nanjing University, Nanjing, Jiangsu 210093, China
[*]E-mail: liuqi62@163.com, liuhj@shu.edu.cn

Received: 21 July 2018 / *Accepted:* 12 September 2018 / *Published:* 5 January 2019

Layered cadmium-based coordination polymer ([Cd(4,4'-bpy)(tfbdc)(H_2O)$_2$], Cd-LCP) nanorods and microblocks were synthesized by a facile hydrothermal method (4,4′-bpy = 4,4′-bipyridine, H_2tfbdc = tetrafluoroterephthalic acid). The Cd-LCP were characterized by IR spectrum, elemental analysis, powder X-ray diffraction, thermogravimetric analysis, scanning electron microscope (SEM), transmission electron microscope (TEM), and the Brunauer−Emmett−Teller (BET) surface. As an anode material of lithium-ion batteries, the Cd-LCP nanorods and microblocks showed a higher reversible capacity and an excellent cyclic stability, maintaining 231 mA h g^{-1} after 50 cycles at 50 mA g^{-1}. Our results further confirm that searching for anode materials of lithium-ion batteries from 2D coordination polymer is an effective route.

Keywords: cadmium compound; coordination polymer; lithium-ion batteries; electrode material

1. INTRODUCTION

Lithium-ion batteries have been widely used in portable electronic devices, due to their high energy density, however, ordinary lithium-ion batteries using the extraction/insertion of Li-ions between lithium transition metal oxide cathode and graphite anode hardly satisfy the need in the field of hybrid electric vehicles (HEVs), electric vehicles (EVs) and smart grid.[1–4] For developing high performance lithium-ion batteries, considerable research work have been centered on the synthesis of new organic-based, inorganic-based and inorganic-organic hybrid electrode materials [5-9]. Besides, considering

sustainable development and environment protection, renewable electrode materials have received considerable attention [10]. For the past ten years, owing to their high surface area, redox activity, controlled pore size and channels, porous coordination polymers constructed by the interactions of metal ions or metal clusters and organic ligands, which is also known as metal-organic frameworks (MOFs), have displayed many potential applications in optical materials, catalysis, gas storage and separation, drug delivery, sensor and energy storage [11-20].

Coordination polymers (CPs) as electrode materials applied in lithium-ion batteries can be classified into two routes. One route is that metal oxides @carbon nanocomposites or nanoscale/nanostructured metal oxides can be synthesized by using CPs as precursors [21-23]. Another route is that CPs can be directly served as electrode materials for lithium-ion batteries, owing to their porosity, offering the diffusion route and storage space of lithium ions, and the redox active metal ions [24-42]. For instance, as the first MOF-based cathode material of lithium-ion batteries, $Fe^{III}(OH)_{0.8}F_{0.2}[O_2C\text{-}C_6H_4\text{-}CO_2]$, having an excellent cycling performance and a lower capacity of 70 mA h g^{-1}, has been reported by Tarascon et al [25]. $[Zn_3(HCOO)_6]$, as an anode material, can deliver a discharge capacity of 560 mA h g^{-1} after 60 cycles at 60 mA g^{-1} [26]. As an anode material, a two dimensional (2D) Mn-based CP ($[Mn(tfbdc)(4,4'\text{-bpy})(H_2O)_2]$) was reported by us, which can deliver a reversible capacity of 390 mA h g^{-1}after 50 cycles [30]. Mahanty et al reported that a Mn-based MOF, as an anode material, can show specific capacity of 694 mA h g^{-1} at 100 mA g^{-1} after 100 cycles and good cycle stability [38]. As an anode material, a bimetallic MOF (Co-Zn-MOF) exhibits high capacity of 1211 mA h g^{-1} at 0.1 and excellent rate capability [40]. Very recently, we synthesized a one dimensional (1D) CP ($[Zn(H_2mpca)_2(tfbdc)(H_2O)]$, Zn-ODCP), and investigated its electrochemical properties as an anode material; Zn-ODCP electrode has a specific capacity of 300 mA h g^{-1} at 50 mA g^{-1} after 50 cycles [41]. Varies of metal-based CPs as electrode materials of lithium-ion batteries have been reported, but, until now, cadmium-based CP as an electrode material of lithium-ion batteries has not been reported. On the other hand, CPs usually have poor electrical conductivity, which is unfavorable for performance improvement of the CP-based electrode. So, like as inorganic nanomaterials reported [43-44], preparing nanosized CP should be a good route for improving the ion transfer rate and electrical conductivity of them. Herein, we synthesized a cadmium-based 2D CP ($[Cd(4,4'\text{-bpy})(tfbdc)(H_2O)_2]$, Cd-LCP) nanorods and microblocks by a facile hydrothermal method via using environmental friendly materials, tetrafluoroterephthalatic acid (H_2tfbdc), 4,4′-bipyridine (4,4′-bpy) and cadmium (II) acetate dehydrate. The structure characterization and the electrochemical performances of Cd−LCP nanorods and microblocks were reported.

2. EXPERIMENTAL

2.1. Materials

Cd(II) acetate dihydrate, tetrafluoroterephthalic acid (H_2tfbdc) and 4,4′-bipyridine (4,4′-bpy) were purchased from Shanghai Chemical Reagent Company. All the reagents were of analytical purity and used without further purification.

2.2. Synthesis of [Cd(4,4'-bpy)(tfbdc)(H_2O)$_2$] (Cd -LCP)

According to the method reported with some modifications, Cd-LCP was synthesized [42, 45]. Tetrafluoroterephthalic acid (0.30 mmol, 0.0714 g), 4,4'-bipyridine (0.30 mmol, 0.0576 g), $Cd(CH_3CO_2)_2 \cdot 2H_2O$ (0.30 mmol, 0.080 g) and H_2O (9 mL) were added into a stainless-steel autoclave with Teflon-lined of 15 mL and heated at 100 °C for 24 h. The white product [Cd(4,4'-bpy)(tfbdc)(H_2O)$_2$] (Cd-LCP) was collected by filtration, washed with water and acetone, and dried in air. Yield: 0.073g, 67% (based on Cd). Before as-synthesized Cd-LCP was served as anode material, it was ground for 2 hr.

2.3. Characterization

Field emission scanning electron microscopy (FESEM) experiments were carried out on a S-4800 field emission SEM system (Hitachi). Powder X-ray diffraction (XRD) measurements were conducted on an X-ray diffractometer with Cu-Kα radiation (λ = 0.15406 nm, D/max 2500 PC, Rigaku). X-ray photoelectron spectrum (XPS) was performed on an ESCALABMK II X-ray photoelectron spectrometer. Fourier transform infrared spectrum (FT-IR) was investigated using a Nicolet 460 spectrophotometer. A Perkin-Elmer 2400 Series II element analyzer was used to measure the elemental analysis (C, H, and N). Under air atmosphere, thermogravimetric analysis (TGA) experiment was performed on a Dupont thermal analyzer from room temperature to 800 ˚C at a heating rate of 10˚C/min. Nitrogen sorption isotherm was carried out at 77 K using a Micromeritics ASAP2010C pore analyzer after as-synthesized Cd-LCP was degassed under vacuum condition for 15 hr at 50 ˚C. The surface area was ascertained by the Brunauer, Emmett, and Teller (BET) equation. The pores size and pore volume were determined by the Barrett, Joyner, and Halenda (BJH) analyses.

2.4. Electrochemical Measurements

The electrochemical performances for the Cd-LCP nanorods and microblocks were investigated by using CR 2016 coin-type half cells. The working electrode was prepared by mixing 60 wt% Cd-LCP nanorods and microblocks, 30 wt% acetylene black and 10 wt% polytetrafluoroethylene (PTFE) in N-methylpyrollidinone (NMP). The resulting slurry was coated onto a copper foil current collector. Coated electrodes were dried at 80 °C in a vacuum oven for 12 h and then pressed. CR 2016 coin-type batteries were assembled in an argon-filled glovebox (Mbraun, Unilab, Germany), using a porous polypropylene as the separator, a lithium-foil as the counter electrode, and 1M $LiPF_6$ in a mixture of ethylene carbonate (EC) and diethyl carbonate (DMC) (V_{EC} : V_{DMC} = 1:1) as the liquid electrolyte. The charge-discharge experiments were carried out on a battery test system (Newwell CT 3008W) in the potential range of 0.01~3 V versus Li/Li^+ at different current rate. In the potential range of 0.1~3V, cyclic voltammogram (CV) was tested at a scanning rate of 0.1 mV/s. Electrochemical impedance spectroscopy (EIS) was measured at the open circuit voltage with an amplitude of 5 mV in 0.01-10^5Hz frequency range. CV and EIS measurements were conducted on a CHI 660D electrochemical workstation. The specific capacity was calculated according to the weight of the Cd-LCP, and expressed in mA h g^{-1}.

3. RESULTS AND DISCUSSION

3.1 Physical Characterization

The powder X-ray diffraction (XRD) pattern of as-synthesized Cd-LCP is displayed in Figure 1a. Compared with the diffraction peak positions of the simulated pattern based on [Zn(4,4'-bpy)(tfbdc)(H_2O)$_2$] (Zn-LCP) single crystal data (CCDC 737134), that of the Cd-LCP are basically consistent with them [45], which reveals the Cd-LCP has a similar molecular formula ([Cd(4,4'-bpy)(tfbdc)(H_2O)$_2$]) with Zn-LCP. Elemental analysis experiment was used to ascertain the composition of the Cd-LCP.

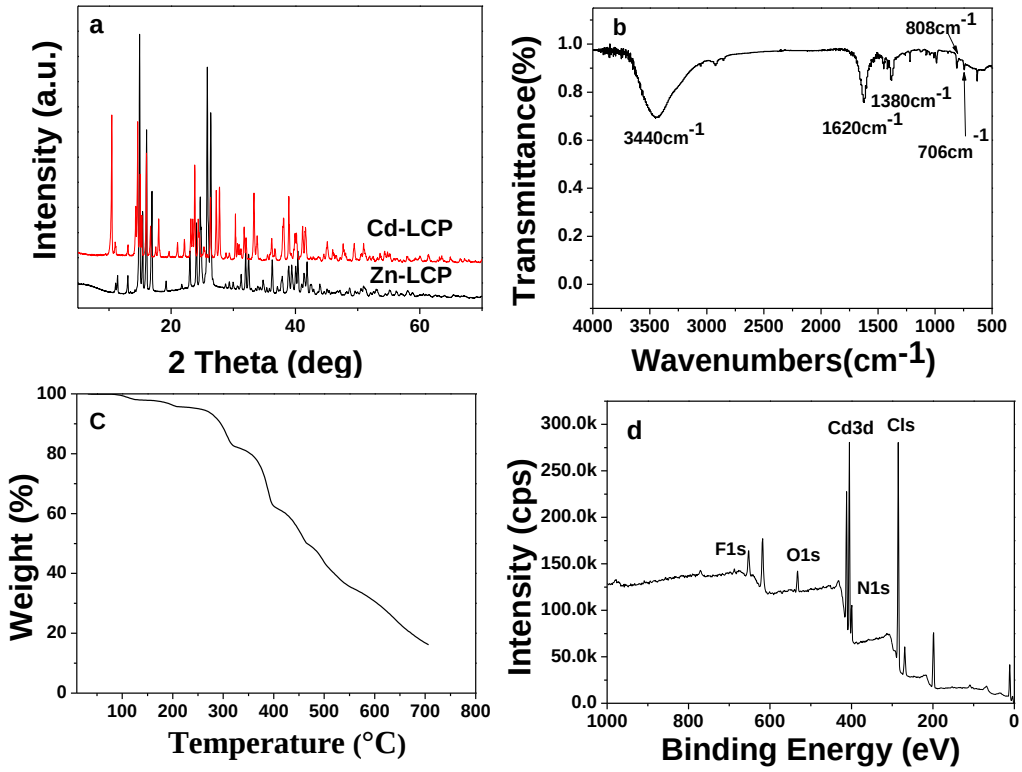

Figure 1. (a) XRD pattern of as-synthesized Cd-LCP and the simulated pattern based on Zn-LCP crystal data. (b) The FT-IR spectrum. (c) Thermal gravimetric analysis graph. (d) XPS survey spectrum of Cd-LCP.

The calculation results of C, H and N (Wt %) according to the formula of Cd-LCP are accorded with the elemental analysis results for the Cd-LCP (Calculation for Cd-LCP: C, 39.98; H, 2.24; N, 5.17; Found: C, 39.33; H, 2.54; N, 5.72), verifying the correction of the formula. From the FT-IR spectrum of the Cd-LCP (Figure 1b), it can be observed that there is a absorption band at ca. 3440 cm^{-1}, belonging to ν(OH) of coordinated water molecules. The strong absorption bands at 1620 and 1380 cm^{-1} are due to the ν_{as}(OCO) and ν_s(OCO) stretching modes of coordinated tetrafluoroterephthalate ($tfbdc^{2-}$) anions, and the absorption peak at ca. 808 cm^{-1} is produced by ν(C−H) bent vibrations of 4,4′-bipy [30]. While the δ(OCO) bent vibration peak from $tfbdc^{2-}$ anions appears at ca. 706 cm^{-1}. Figure 1c is thermal

gravimetric analysis graph for the Cd-LCP. From Figure 1c, the weight decrease of Cd-LCP from 89 to 276˚C is 6.7 %, due to the two coordinated water molecules losing (calculated 6.65 %), the weight decrease from 276 to 400˚C should be ascribed to one 4,4′-bipy molecule losing (calculated 28.48%, found 30.91 %), then, the remaining matter is gradually decomposed at more than 400˚C. Figure 1d is the survey spectrum of the Cd-LCP. From it, we can observe that the peaks of Cd, C, N, O and F all appear, ascertaining the Cd-LCP consists of Cd, C, N, O and F elements. The binding energies of C 1s, N 1s, O 1s, F 1s and Cd 3d 5/2and the 3d3/2 orbit are 284.86, 398.62, 530.73, 686.48, 405.30 and 412.08 eV, respectively, as shown in Figure S 1a-e (supporting information), which is consistent with the value reported [46].

The microstructure and morphology of the Cd-LCP material were investigated by Field emission scanning electron microscopy (FESEM). Low magnification and higher magnification FESEM images of the Cd-LCP are shown in Figure 2a and Figure 2b-d, respectively. From Figure 2b, it can be seen that the Cd-LCP sample is composed of many nanorods and microblocks. While the microblock is also consist of nanosheets (Figure 2c). The length, width, and thickness of nanorods are 0.5− 4 um, 400−600 nm and 40−150 nm, respectively (Figure 2b, c).

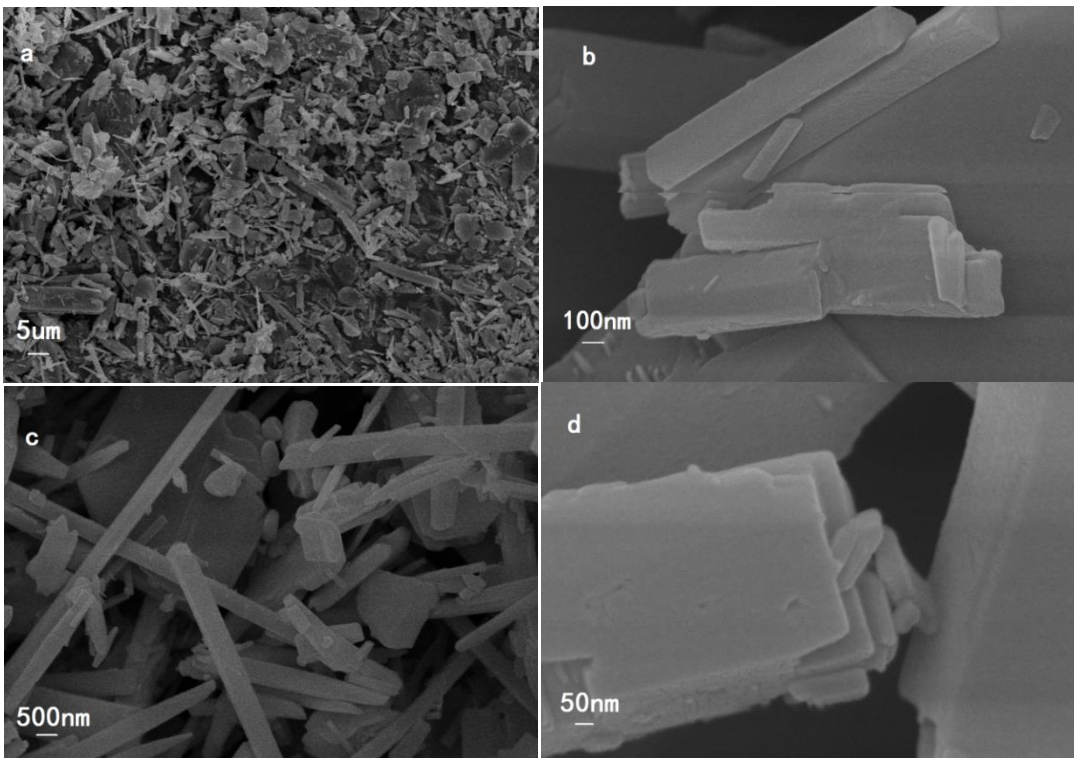

Figure 2. FESEM images of the Cd-LCP nanorods and microblocks: (a) Low magnification, (b-d) higher magnification.

Same with the structure of [Zn(4,4'-bpy)(tfbdc)(H_2O)$_2$], Cd-LCP is also a 2D layered coordination polymer, as presented in Figure 3a. These 2D layers are packed into a 3D supramolecular network via the interactions of hydrogen bonds [45].

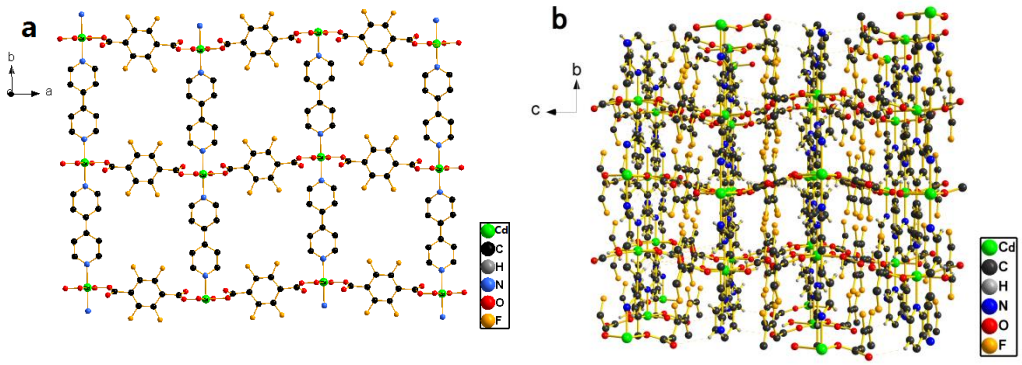

Figure 3. (a) 2D structure of Cd-LCP. Hydrogen atoms are omitted for clarity, (b) 3D structure of Cd-LCP.

Cd-LCP can be acted as a candidate for electrode material for lithium-ion batteries, owing to the 2D layered coordination polymers can provide redox active metal ions and interspaces of the layers for the diffusion of electrolyte ions.

As shown in Figure 4, isotherm of the Cd-LCP is attributed to the type between II and III. Hysteretic loop in the range of 0.65-1.0 P/P_0 is ascribed to a type of H_3 hysteresis. The BET surface area and total pore volume of the Cd-LCP sample are 16.28 $m^2 g^{-1}$ and 0.0072 $cm^3 g^{-1} nm^{-1}$. The pore size distribution curve is shown in the inset of Figure 4. From Figure 4, it can be observed that there are not only micropores, but also mesopores and macropores in the Cd-LCP sample. The mesopores and macropores belong to interparticle pores, and micropores should belong to the structural pore of the Cd-LCP itself. Such pore structure makes the Cd-LCP potentially acted as an electrode material, owing to it being favorable to the diffusion and storage of electrolyte solution [47].

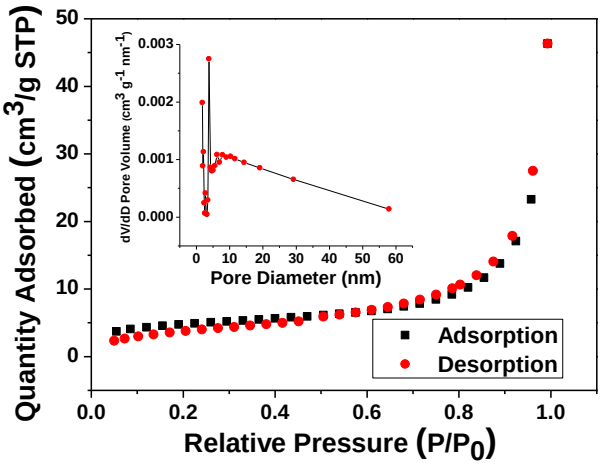

Figure 4. N_2 adsorption–desorption isotherm of the Cd-LCP sample (inset is pore size distribution curve)

3.2 Electrochemical performance

The four successive cyclic voltammetry (CV) scan curves of the Cd-LCP nanorods and microblocks in the range of 0.1-3.0 V is presented in Figure 5a. During the first cathodic scan, the

consumption of the coordinated water molecules may result in the production of the peak at 1.72 V, the formation of a solid electrolyte interface (SEI) film is related with the production of the peak at 1.01 V, and the conversion of Cd-LCP to a Cd/[Li_2(4,4′-bpy)(tfbdc)] nanocomposite may result in the production of the peak at 0.44 V. In the first anodic scan, the peak produced by oxidation of metal Cd(0) to Cd(II) appears at 1.05 V [48]. While in the second scan, due to the structure arrangements and some side reactions in the first scan, only the peak at 0.57 V appears. This phenomenon has appeared in other CPs based electrodes [30-34]. After the second scan, the CV curves were almost overlapped, affirming the excellent reversibility and stability of the Cd-LCP electrode.

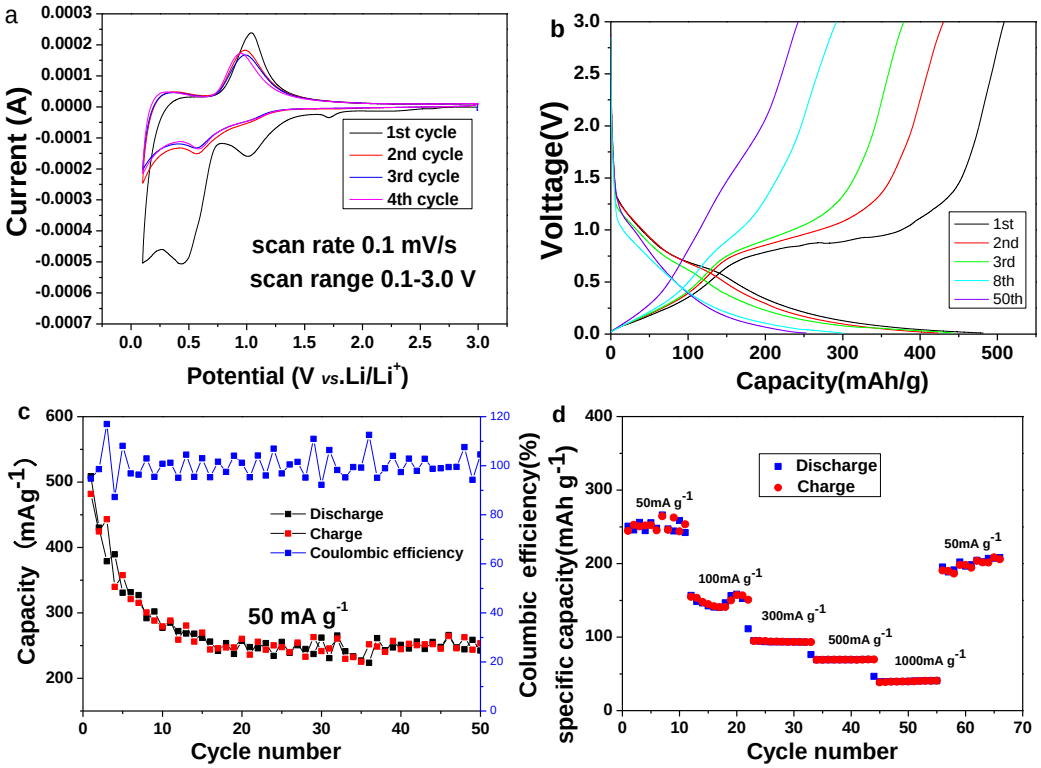

Figure 5. (a) CV curves of the Cd-LCP nanorods and microblocks electrode (b) Charge/discharge profiles of the Cd-LCP nanorods and microblocks electrode between 0.01-3.0V at a current density of 50 mA g^{-1}. (c) Cycling performances (d) Rate performances.

According to the analysis for CV curves above mentioned and related reports about MOF based-electrode [26], the following equation can be used to express the possible conversion reaction in the Cd-LCP nanorods and microblocks electrode:

$$[Cd(4,4'\text{-}bpy)(tfbdc)] + 2Li^+ + 2e \longleftrightarrow Cd + [Li_2(4,4'\text{-}bpy)(tfbdc)]$$

As displayed in above equation, Cd-LCP reacts with Li by conversion reaction in the first discharge process, resulting in the formation of [Li_2(4,4′-bpy)(tfbdc)] and Cd.

A few charge/discharge curves for the Cd-LCP nanorods and microblocks electrode at a current density of 50 mA g^{-1} are exhibited in Figure 5b. A gently plateau appears as the voltage decreases to ca. 0.75 V from the open circuit voltage, and then it decreases slowly to 0.01 V, owing to the SEI layer formation, the reduction of Cd (II) to Cd (0) and some side-reactions. The discharge capacities of the

first and the second cycle for Cd-LCP nanorods and microblocks electrode are 481.2 mA h g^{-1} and 424.9 mA h g^{-1}, respectively. The irreversible capacity loss (ICL) is 11.69%. The production of a SEI film on the electrode and the electrolyte decomposition result in this loss [30, 49, 50]. The cycling performance and coulumbic efficiency *versus* cycle number at 50 mA g^{-1} is shown in Figure 5c. The capacity decay produced by the irreversible structure transformation and complicated side-reactions can be observed in the first cycle. After the 9th cycle, the Cd-LCP electrode keeps basically a steady reversible capacity. The discharge capacities of the 10th and the 40th cycle are 279 and 244 mA h g^{-1}, respectively. The discharge capacity is kept at 254 mA h g^{-1} after 50 cycles. Although this capacity is lower than that of some MOF based anode materials reported (Table 1), the results mentioned above show clearly that the Cd-LCP electrode has good cycling stability. In the first cycle, the coulombic efficiency of the Cd-LCP nanorods and microblocks is about 94.70%, and then it gradually increases to 104.56% in the 50th cycle (Figure 5c). Figure 5d presents the rate-performance of the Cd-LCP electrode. When the current density is at 50, 100, 300, 500 and 1000 mA g^{-1}(each for 11 cycles), the capacities of average 244, 149, 95, 71 and 41 mA h g^{-1} are obtained, respectively. As the current density is returned to 50 mA g^{-1}, the capacity is also returned to 205 mA h g^{-1}.

Table 1. Specific capacitance of the Cd-LCP electrode in this study, compared with some MOF/CP-based electrodes reported in previous literature

MOF/CP	Specific Capacity (mA h g^{-1})	Current Density (mA g^{-1})	Cycle number	Initial Coulombic efficiency (%)	Voltage (V vs. Li/Li^+)	Ref.
MOF-177	105	50	50	26.3	0.05-1.6	24
$Zn_3(HCOO)_6$	520	60	60	97	0.005-3	26
Mn(tfbdc)(4,4-bpy)$(H_2O)_2$	390	50	50	30.5	0.1-3	30
$Co_2(OH)_2BDC$	650 and 210	50 and 500	100	72.8	0.02-3	32
Mn(3,5-PDC)·$2H_2O$	554	100	240	60	0.05-3	34
$Zn(IM)_{1.5}(abIM)_{0.5}$	190 and 75	100 and 400	200	53	0.01-3	35
Asp-Cu	233 and 125	50 and 400	100	26.6	0.01-3.0	37
Mn-BTC	694 and 400	103 and 1030	100	40	0.01-2.0	38
Cd(4,4'-bpy)(tfbdc)$(H_2O)_2$	254	50	50	88.31	0.01-3	This work

The following factors result in the better performance of the Cd-LCP nanorods and microblocks electrode: first, the Cd-LCP has the layered structure feature, in which excepting Cd^{2+} ion can take part in the conversion reaction, tetrafluoroterephthalate anion can also involve electron transfer process, like as reported terephthalate lithium [10]; second, the Cd-LCP nanorods and microblocks have higher surface area and smaller size, which can provide more electrochemical reaction sites and shorten the

diffusion pathway of Li-ion; third, the pore structure feature with micropores, mesopores and macropores of the Cd-LCP.

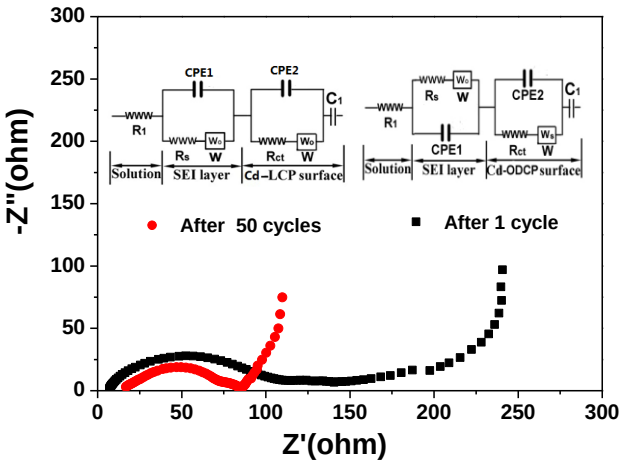

Figure 6. The Nyquist curves of the Cd-LCP electrode after 1 and 50 cycle.

Electrochemical impedance spectroscopy (EIS) was used to evaluate electrochemical behavior of the Cd-LCP nanorods and microblocks electrode. Figure 6 presents two Nyquist ac impedance plots of the Cd-LCP nanorods and microblocks. Each plot contains two parts, one is an inclined line, and the other is two partially overlapped semicircles. The semicircle produced by the SEI passivating film locates at high frequency, and the other semicircle from the charge transfer process appears at high-middle frequencies [39, 51]. For fitting the impedance data, two equivalent circuit models were used, as displayed in inset of Figure 6. Table 2 presents the fitted values produced by Zview software. It can be seen that the ionic resistance of the electrolyte (R_l) after 1 cycle is 6.3 Ω, lower than 11.4 Ω after 50 cycles, meaning the Cd-LCP nanorods and microblocks electrode has good stability. R_{ct}, $R_{s,}$ as well as Q1 and Q2 stands for charge transfer resistance, the SEI passivating film resistance, and CPE constant phase elements, respectively. The R_{ct} of the electrode after 50 cycles is 47.1 Ω, lower than 70.8 Ω after 1 cycle. This result may be related to the better wetting of the Cd-LCP electrodes and improved connectivity [38].

Table 2. The fitted data for impedance spectra after 1 and 50 cycle

sample	*R*1	*R*s	CPE1-T	CPE1-P	*W1*-R	R_{ct}	*W2*-R	CPE2-T	CPE2-P	*C1*
after 1 cycle	6.3	25.2	5.9×10^{-6}	0.91	1.8×10^{-3}	70.8	56.4	0.91	1.0×10^{-4}	1.65
after 50 cycles	11.4	13.6	7.3×10^{-3}	0.21	2.6×10^{-15}	47.1	0.48	4.1×10^{-5}	0.69	1.1×10^{12}

4. CONCLUSIONS

In summary, layered cadmium-based coordination polymer [Cd(4,4'-bpy)(tfbdc)(H_2O)$_2$] (Cd-LCP) nanorods and microblocks were successfully synthesized by a facile hydrothermal treatment. As

an anode material of lithium-ion batteries, the Cd-LCP nanorods and microblocks still maintained a capacity of 254 mA h g^{-1} after 50 cycles, and showed a good cycling stability. This is the first report that cadmium-based coordination polymer as an electrode material for lithium-ion batteries. This research further confirms 2D coordination polymer can serve as electrode materials for lithium-ion batteries. The related study of finding more 2D coordination polymers based electrode materials is under way in our laboratory.

SUPPORTING INFORMATION:

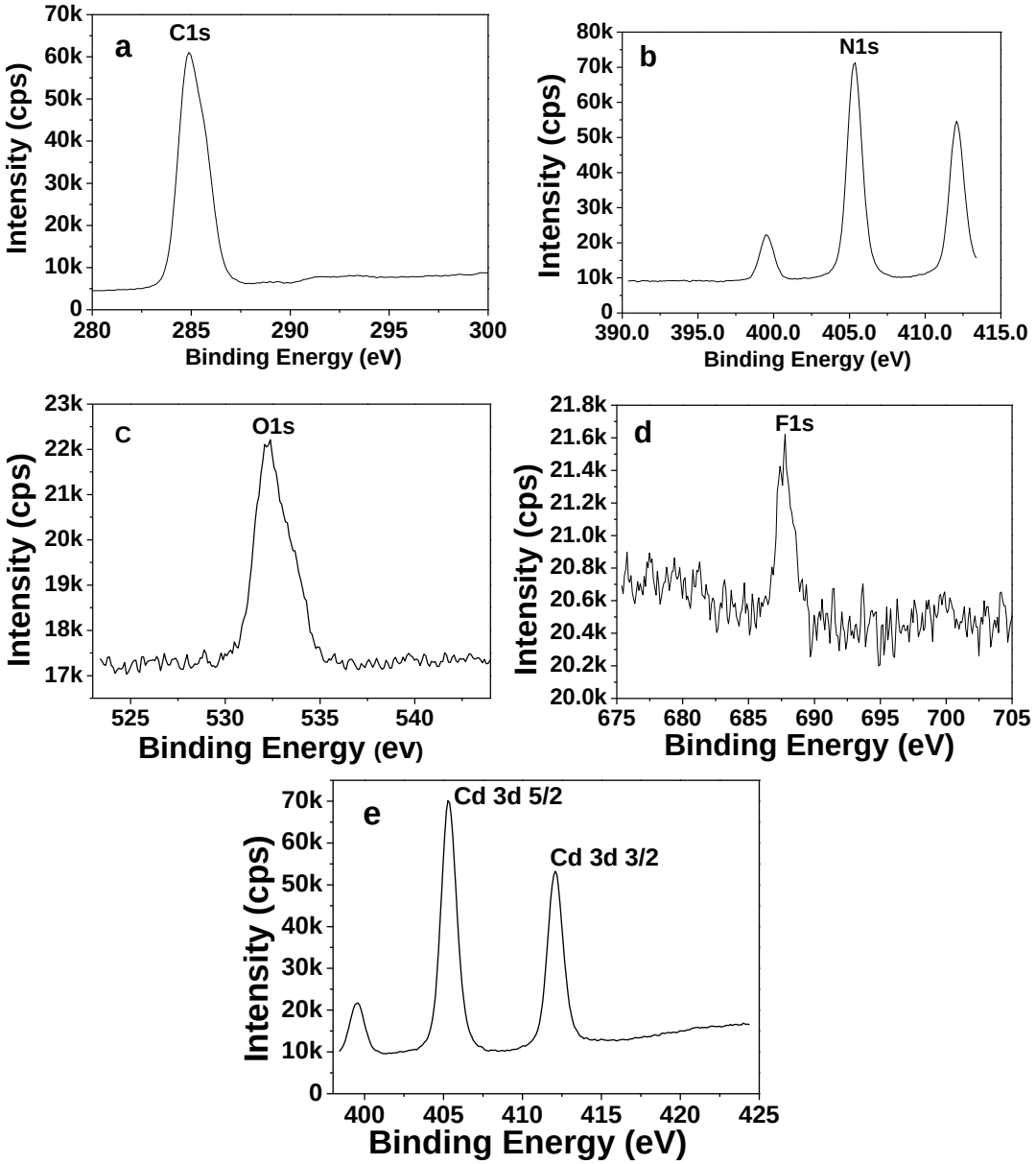

Figure S 1. (a-e) XPS core level spectra of C 1s, N 1s, O 1s, F 1s and Cd 3d of Cd-LCP.

ACKNOWLEDGEMENTS
We thank the financial support from the National Natural Science Foundation of China (No. 20971060), the Natural Science Research Key Project of Jiangsu Colleges and Universities (No. 16KJA430005), Jiangsu Province Key Laboratory of Fine Petrochemical Engineering and the Natural Science Foundation of State Key Laboratory of Coordination Chemistry.

References

1. M.S. Whittingham, *Chem. Rev.,* 114 (2014) 11414-11443.
2. J.B. Goodenough, K.S. Park, *J. Am. Chem. Soc.,* 135 (2013) 1167-1176.
3. R.V. Noorden, *Nature,* 507 (2014) 26-28.
4. D. Larcher, J.M. Tarascon, *Nat. Chem.,* 7 (2015) 19-29.
5. N. Ogihara, T. Yasuda, Y. Kishida, T. Ohsuna, K. Miyamoto, N. Ohba, *Angew. Chem. Int. Ed.,* 53 (2014) 11467-11472.
6. J.B. Goodenough, Y. Kim, *Chem. Mater.,* 22 (2010) 587-603.
7. L. Wang, Y.Z. Han, X. Feng, J.W. Zhou, P.F. Qi, B. Wang, *Coord. Chem. Rev.,* 307 (2016) 361-381.
8. Z.P. Song, Y.M. Qian, M.L.Gordin, D.H. Tang, X. Terrence, M. Otani, H. Zhan, H.S. Zhou, D.H. Wang, *Angew. Chem.,* 127 (2015) 14153-14157.
9. Y. Liang, Z. Tao, J. Chen, *Adv. Energy Mater.,* 2 (2012) 742-769.
10. M. Armand, S. Grugeon, H. Vezin, S. Laruelle, P. Ribiere, P. Poizot, J.M. Tarascon, *Nat Mater.,* 8 (2009) 120-125.
11. L.E. Kreno, K. Leong, O.K. Farha, M. Allendorf, R.P.V. Duyne, J.T. Hupp, *Chem. Rev.,* 112 (2012) 1105-1125.
12. H. Furukawa, K.E. Cordova, M.O. Keeffe, O.M. Yaghi, *Science,* 341 (2013) 974-986.
13. J.S. Seo, D. Whang, H. Lee, S.I. Jun, J. Oh, Y.J. Jeon, K. Kim, *Nature,* 404 (2000) 982-986.
14. X.M.Wang, X.X. Liu, H.R. Rong, Y.D. Song, H. Wen, Q. Liu, *RSC Adv.,* 7 (2017) 29611-29617.
15. A. Morozan, F. Jaouen, *Energy Environ. Sci.*, 5 (2012) 9269-9290.
16. H.Y. Wang, Y. Wu, C.F. Leong, D.M. D'Alessandro, J.L. Zuo, *Inorg. Chem.,* 54 (2015) 10766-10775.
17. Q. Liu, X.X. Liu, C.D. Shi, Y.P. Zhang, X.J. Feng, M.L. Cheng, S. Su, J. Gu, *Dalton Trans.,* 44 (2015) 19175-19184.
18. X.X. Liu, C.D. Shi, C.W. Zhai, M.L. Cheng, Q. Liu, G. Wang, *ACS. Appl. Mater. Interfaces,* 8 (2016) 4585-4591.
19. F.S. Ke, Y.S. Wu, H.X. Deng, *J. Solid State Chem.,* 223 (2015) 109-121.
20. L.L. Yu, X.M. Wang, M.L. Cheng, H.R. Rong, Y.D. Song, Q. Liu, *Cryst. Growth Des*., 18 (2017) 280-285.
21. Z.C. Bai, Y.H. Zhang, Y.W. Zhang, C.L. Guo, B. Tang, D. Sun, *J. Mater. Chem. A,* 3 (2015) 5266-5269.
22. S.J. Yang, S. Nam, T. Kim, H.I. Ji, H. Jung, J.H. Kang, S. Wi, B. Park, C.R. Park, *J. Am. Chem. Soc.,* 135 (2013) 7394-7397..
23. F. Zou, X.L. Hu, Z. Li, L. Qie, C.C. Hu, R. Zeng, Y. Jiang, Y.H. Huang, *Adv. Mater.,* 26 (2014) 6622-6628.
24. X.X. Li, F.Y. Cheng, S.N. Zhang, Chen. J, *J. Power Sources,* 160 (2006) 542-547.
25. G. Ferey, F. Millange, M. Morcrette, C. Serre, M.L. Doublet, J.M. Greneche, J.M. Tarascon, *Angew. Chem. Int. Ed.,* 46 (2007) 3259-3263.
26. K. Saravanan, M. Nagarathinam, P. Balaya, J.J. Vittal, *J. Mater. Chem.,* 20 (2010) 8329-8335.
27. M. Nagarathinam, K. Saravanan, E.J.H. Phua, M.V. Reddy, B.V.R. Chowdari, J.J. Vittal, *Angew. Chem.,* 124 (2012) 5968-5972.
28. J.F. Xiang, C.X. Chang, M. Li, S.M. Wu, L.J. Yuan, J.T. Sun, Cryst. *Growth Des.,* 8 (2008) 280-

282.
29. Y. Mao, Q.Y. Kong, B.K. Guo, X.P. Fang, X.W. Guo, L. Shen, M. Armand, Z.X. Wang, L.Q. Chen, *Energy Environ. Sci.,* 4 (2011) 3442-3447.
30. Q. Liu, L.L. Yu, Y. Wang, Y.Z. Ji, J. Horvat, M.L. Cheng, X.Y. Jia, G.X. Wang, *Inorg. Chem.,* 52 (2013) 2817-2822.
31. Z.Y. Zhang, H. Yoshikawa, K. Awaga, *J. Am. Chem. Soc.,* 136 (2014) 16112-16115.
32. L. Gou, L.M. Hao, Y.X. Shi, S.L. Ma, X.Y. Fan, L. Xu, D.L. Li, K.J. Wang, *J. Solid State Chem.,* 210 (2013) 121-124.
33. L. Tang, S. Zhang, G.M. Zeng, Y. Zhang, G.D. Yang, J. Chen, J.J. Wang, J.J. Wang, Y.Y. Zhou, Y.C. Deng, *J. Colloid Interface Sci.,* 445 (2015) 1-8.
34. H.L. Fei, X. Liu, Z.W. Li, W.J. Feng, *Dalton Trans.,* 44 (2015) 9909-9914.
35. Y.C. Lin, Q.J. Zhang, C.C. Zhao, H.L. Li, C.L. Kong, C. Shen, L. Chen, *Chem. Commun.,* 51 (2015) 697-699.
36. W. Kaveevivitchai, A.J. Jacobson, *J. Power Sources,* 278 (2015) 265-273.
37. C.C. Zhao, C. Shen, W.Q. Han, *RSC Adv.,* 5 (2015) 20386-20389.
38. S. Maiti, A. Pramanik, U. Manju, S. Mahanty, *ACS. Appl. Mater. Interfaces,* 7 (2015) 16357-16363.
39. C.D. Shi, Q.H. Xia, X. Xue, Q. Liu, H.J. Liu, *RSC Adv.,* 6 (2016) 4442-4447.
40. C. Li, X.S. Hu, X.B. Lou, Q. Chen, B.G. Hu, *Chem. Commun.,* 52 (2016) 2035-2038.
41. Y.D. Song, L.L. Yu, Y.R. Gao, C.D. Shi, M.L. Cheng, X.M. Wang, H.J. Liu, Q. Liu, *Inorg. Chem.,* 56 (2017) 11603-11609.
42. C.D. Shi, X.M. Wang, Y.R. Gao, H.R. Rong, Y.D. Song, H.J. Liu, Q. Liu, *J. Solid State Electrochem.,* 21 (2017) 2415-2423.
43. S.Q. Chen, W.K. Yeoh, Q. Liu, G.X. Wang, *Carbon,* 50 (2012) 4557-4565.
44. L. Zhang, H.B. Wu, S. Madhavi, H.H. Hng, X.W. Lou, *J. Am. Chem. Soc.,* 134 (2012) 17388-17391.
45. Z. Hulvey, E. Ayala, A.K. Cheetham, *Z. Anorg. Allg. Chem.,* 635 (2009) 1753-1757.
46. S.H. Liu, D.H. Wang, C.H. Pan, *Analysis of X-ray Photoelectron Spectroscopy*, Science Press, Beijing, (1988).
47. H.Q. Cao, B.J. Li, J.X. Zhang, F. Lian, X.G. Kong, M.Z. Qu, *J. Mater. Chem.,* 22 (2012) 9759-9766.
48. J.K. Feng, S.L. Xiong, Y.T. Qian, L.W. Yin, *Electrochim. Acta,* 129 (2014) 107-112.
49. L.L. Xu, S.W. Bian, K.L. Song, *J. Mater. Sci.,* 49 (2014) 6217-6224.
50. B. Sun, J. Horvat, H.S. Kim, W-S. Kim, J. Ahn, G. Wang, *J. Phys. Chem. C,* 114 (2010) 18753-18761.
51. Y.D. Ko, J.G. Kang, J.G. Park, D.W. Kim, *J. Appl. Electrochem.,* 40 (2009) 109-114.